Working with a computational model for high frequency stimulation

Alejandro Pascual

INRIA

INSTITUT NATIONAL DE RECHERCHE EN INFORMATIQUE ET EN AUTOMATIQUE

Working with a computational model for high frequency stimulation

Alejandro Pascual

N° 5890

Avril 2006

Thème BIO

ISSN 0249-6399 ISRN INRIA/RR--5890--FR+ENG

Working with a computational model for high frequency stimulation

Alejandro Pascual*

Thème BIO — Systèmes biologiques
Projet ANUBIS
Scientific leader: Jacques Henry

Rapport de recherche n° 5890 — Avril 2006 — 32 pages

Abstract: Despite real therapeutic successes, the fundamental physiological mechanisms underlying the effect of deep brain stimulation are still not understood. Several attempts have been made to explore these mechanisms with computational models. Unfortunately so far mathematical models have not had a significant impact on mainstream research on deep brain stimulation in Parkinson's disease. In this paper we report our internship experience working with a computational model proposed by Rubin and Terman in 2004 [1] which is among the most realistic and comprehensive models published recently.

Key-words: deep brain stimulation, high frequency stimulation, Parkinson's disease, computational model, tremor

* E-mail address: alepasc@adinet.com.uy

Unité de recherche INRIA Futurs
Parc Club Orsay Université, ZAC des Vignes,
4, rue Jacques Monod, 91893 ORSAY Cedex (France)
Téléphone : +33 1 72 92 59 00 — Télécopie : +33 1 72 92 59 ??

Etude d'un modèle informatique de la stimulation cérébrale de haute fréquence

Résumé : Malgré des succès thérapeutiques réels, les mécanismes physiologiques fondamentaux sous-tendant l'effet de la stimulation cérébrale profonde ne sont toujours pas compris. Plusieurs essais ont été faits pour explorer ces mécanismes avec des modèles informatiques. Malheuresusement pour l'instant ces modèles informatiques n'ont pas eu d'impact significatif sur la recherche principale sur la stimulation cérébrale profonde dans la maladie de Parkinson. Dans ce papier nous décrivons notre expérience de stage sur l'étude d'un modèle proposé par Rubin et Terman en 2004 [1] qui est parmi les modèles les plus réalistes et les plus complets publiés récemment.

Mots-clés : stimulation cérébrale profonde, stimulation de haute fréquence, maladie de Parkinson, modèle informatique, tremblement

1 Introduction

The use of neuromodulation in general and DBS (Deep Brain Stimulation) in particular, in alleviating symptoms has become a well recognized standard procedure not only in Parkinson's disease (PD), but also in other neurological and psychiatric disorders. Since the pioneer work of Benabid et al. 1987 [2], 1991 [3], new applications of HFS have been proposed regularly (Chang 2004 [4]). Despite these therapeutic successes, the fundamental physiological mechanisms underling the effect of DBS on neural function are still not well understood.

In an effort to understand these mechanisms, several attempts have been made to mathematically model parkinsonian tremor and DBS (for a review see Titcombe et al. 2004 [5]). Early modeling attempts provided little evidence that new models were constructed from previous ones. There are few, if any, citations between papers indicating an awareness of other modeling approaches. It is unlikely that until recently, mathematical models have yet had a significant impact on mainstream research on PD and DBS. As the quality of physiological information relevant to PD is improving, modeling is becoming more focused on the known changes in neuronal activity in the brain and therefore more relevant (Titcombe et al. 2004 [5]).

DBS is also refered to as HFS (High Frequency Stimulation) because its therapeutic effects are only achieved at "high" frequencies (more than $100\,Hz$). In 2004 Rubin and Terman [1] proposed a mechanism for HFS in PD based on single compartment Hodgkin-Huxley-like cell models for four interconnected subcortical nuclei. This model is one of the first to propose an explanation for the reduction of parkinsonian symptoms under HFS, based on *increasing* firing rates in target cells, rather than shutting them down; in agreement with recent experiments that support the former hypothesis (Garcia 2005 [8]).

In this paper we report our experience working with Rubin and Terman's computational model. Simulation results are commented and full mathematical details of the model are explicitly documented in the appendix.

All simulations, were performed using XPPAUT, a software developed by G. B. Ermentrout [17] and available at Ermentrout's home page:
http://www.pitt.edu/ phase/. The numerical method used for integration was an adaptive-step fourth order Runge-Kutta method (Qualst.RK4 in XPPAUT) with a maximum time step of $0.01\,ms$. The model's mathematical details were extracted from an XPPAUT (.ode) file generously provided by David Terman. We took this file as our main reference to the model's details and we documented them in the appendix.

2 Description of Rubin and Terman's model

Four anatomical nuclei are represented in the model: external segment of globus pallidus (GPe), subthalamic nucleus (STN), internal segment of globus pallidus (GPi) and thalamus; where the first three nuclei belong to the basal ganglia (BG). Each of these structures is modeled with a certain number of identical Hodkin-Huxley-like neuron models. Each neuron model consists of a set of ordinary differential equations, that sum up a total of

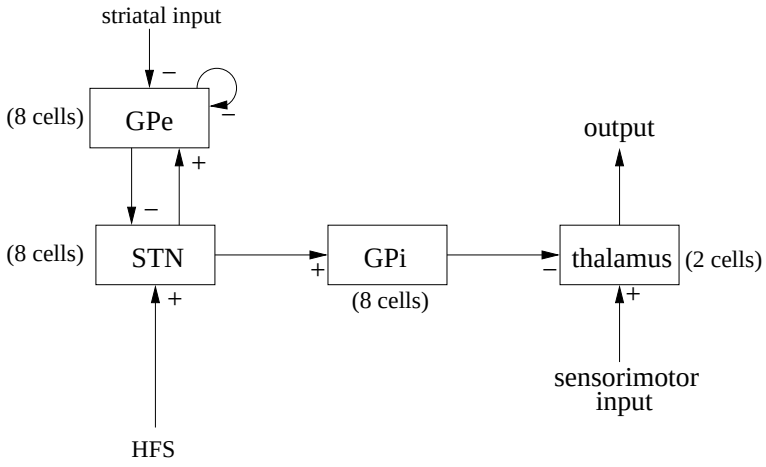

Figure 1: Structures included in the model network. Arrows with "-" signs indicate inhibitory synaptic connections and inputs, while arrows with "+" signs indicate excitatory synaptic connections and inputs. HFS denotes High Frequency Stimulation, which is applied to subthalamic nucleus (STN) in some simulations.

150 coupled non-linear equations for the complete model. More than 100 parameters values are needed to completely specify these differential equations. Inhibitory and excitatory synaptical connections between cells of different nuclei or between cells of the same nucleus (for the only case of GPe), give rise to the block diagram illustrated in figure 1, where several individual connections of the same kind (i.e. inhibitory or excitatory) are grouped together under a single arrow representation. Figure 1 reproduces de block diagram of the computational model we extracted from the XPPAUT file we were provided. However, some differences beetwen the extracted model and the one reported by Rubin and Terman [1] should be noted. First, the block diagram reported in [1] includes connections from GPe to GPi that are not present in the file we were provided. Second, the number of cells reported for each structure in [1] are: 16 for GPe, 16 for STN and 16 for GPi; while in the provided file are: 8 for GPe, 8 for STN and 8 for GPi (as shown in figure 1). Third, the way in which synapses from STN to GPi are modeled in the provided file, differs from the one reported in [1] (we come back to this difference in section 3).

Functionally, the thalamus is viewed simply as a "relay station" where cells have the unique role of responding faithfully to each excitatory sensorimotor afferent action potential (see "sensorimotor input" in figure 1), even under the inhibitory influence of GPi activity.

Rubin and Terman consider two clinical states: "normal" and "parkinsonian" as different states of the BG. Each of these states is characterized by a certain pattern of activity in the output nucleus of the BG (GPi in the model), that determines the responsiveness of thalamic cells to sensorimotor incoming pulses. Performing numerical simulations, Rubin

and Terman [1] have shown the characteristics of these patterns of activity and their effect on thalamic cells responsiveness.

In a "normal" state, output from GPi is irregular and uncorrelated among subpopulations of GPi neurons. It turns out that this has a minimal effect on the responsiveness of thalamic cells. In a "parkinsonian" state, GPi neurons fire bursts of action potentials at 3–8 Hz (which corresponds to tremor frequency). Morover, these bursts are synchronized among subpopulations of GPi neurons. The resulting effect on thalamic cells of this *phasic* inhibition, is that they are no longer able to transmit depolarizing signals faithfully.

The switching from the "normal" state to the "parkinsonian" state is controlled in the model by two GPe parameters: a constant current [1] I_{app}^{GPe} applied to each GPe cell (modeling the level of striatal inhibition to GPe) and a synaptic conductance $g_{GPe \to GPe}$ between pairs of GPe cells. In 2002 Terman, Rubin, Yew and Wilson [6] showed with a computational model, how the combination of weakened intra-GPe inhibitory connections and strengthened striatal inhibition in a structured sparsely-connected coupling architecture between STN and GPe, can set the stage for synchronous GPe-STN oscillations and correlated rhythmic STN output, in a sort of "tremor-like" activity. Their modeling approach to the normal and pathological states of the BG, was motivated by Plenz and Kitai's studies of basal ganglia organotypic tissue cultures (Plenz and Kitati 1999 [7]). These authors propose that the STN and GPe constitute a central pacemaker modulated by striatal inhibition of GPe neurons and that this pacemaker should have far-reaching implications for basal ganglia function and dysfunction. In the complete computational model, with GPi and thalamus included (Rubin and Terman 2004 [1]), when set to the "parkinsonian" state, the correlated rhythmic output of STN leads to rhythmic and synchronous bursting among GPi subpopulations that negatively affects thalamic cells responsiveness to sensorimotor depolarizing signals.

In this scenario HFS is assumed to be an *excitatory* input identically applied to each STN neuron and leads to a new pattern of GPi activity in which GPi cells fire at high frequency (indeed higher than the irregular firing of the "normal" state and the rhythmic bursting of the "parkinsonian" state). Interestingly, the new *tonic* pattern of thalamic inhibition restores the ability of the thalamus to relay sensorimotor input signals faithfully. The explanation given by Rubin and Terman [1] relies on the intrinsic properties of the thalamic cells (particularly the dynamics of a low-threshold T-type Ca^{2+} current) under the effect of different activity patterns of inhibition.

It should be noted that this explanation of how HFS may achieve a therapeutic effect runs counter to much of the existing literature in the field. As it was mentioned before, HFS is supposed to *increase* activity (Garcia 2005 [8]) in the stimulated nucleus (STN) and this leads to increased *tonic* activity in GPi. This is certainly opposed to the view of HFS as a way of *silencing* the pathologically overactive indirect pathway of the BG, as it is the case in a therapeutic lesion (Olanow et al. 2000 [10]). Indeed, the goal of Rubin and Terman's work [1] was to demonstrate, with a computational model, the hypothesis that high firing rates in the output nucleus of the BG caused by HFS, is not contradictory with restoring

[1] Other constant currents are also applied to STN, GPe and GPi cells but they are not represented in figure 1 because they are not used to switch between "normal" and "parkinsonian" states.

thalamic relay function; as it might be though when arguing in terms of *firing rates* and not *patterns* of neuronal activity. In their model, the proposed mechanism for HFS is a natural consequence of the properties of the cells involved.

3 HFS effectiveness dependence on stimulation parameters

We performed simulations to examine the effect of HFS of STN for different levels of HFS amplitude, frequency and pulse widths. More precisely, we numerically studied the dependence of two performance socres that quantify the capability of thalamus to relay a periodic depolarizing input, with respect to the three adjustable HFS parameters.

For the study of the dependence of HFS effectiveness on stimulation parameters, we simulated the HFS signal as a depolarizing periodic smoothed square wave current applied to each STN cell model (see appendix for details). We simulated the full model varying the following stimulation parameters (same values as reported by Rubin and Terman [1]):

- pulse amplitude: $I_{HFS}^{STN} \in \{0, 21.43, 42.86, 64.29, 85.71, 107.1, 128.6, 150.0, 171.4, 192.9, 214.3, 235.7, 257.1, 278.6, 300.0\}\ \frac{pA}{(\mu m)^2}$;
- period: $T_{HFS}^{STN} \in \{3.00, 6.00, 20.0, 40.0\}\, ms$ so that stimulation frequency $f_{HFS}^{STN} \in \{25.0, 50.0, 167, 333\}\, Hz$; and
- pulse duration: $w_{HFS}^{STN} \in \{0.150, 0.300, 0.600, 0.900\}\, ms$.

Optimal clinical results are obtained, on an empirical basis, setting the parameters of the implanted stimulator to (Garcia et al. 2005 [8]): $1 - 5\, V$ (amplitude), $120 - 180\, Hz$ (frequency) and $0.060 - 0.200\, ms$ (pulse duration). Selected stimulation frequencies for simulations ranged over therapeutic ("high" frequency) and non-therapeutic ("low frequency") ranges. Pulse durations were larger than the ones used for optimal clinical results, except for the case $w_{HFS}^{STN} = 0.150\, ms$. This however, allowed us to use a maximum integration step at least ten times smaller than the minimum pulse duration, while still being able to perform simulations on an ordinary personal computer. Current density at a distance of $1\, mm$ from a Medtronic 3387 macroelectrode used for human HFS with a surface area of $6\, mm^2$ passing a current of $3\, mA$, is estimated to be $250\, \frac{pA}{\mu m^2}$ (Lozano 2002 [18]). The range of stimulation amplitude used for simulations was in this order of magnitude.

Each of the 150 state-variables of the model were initialized to zero at $t = 0$. After five seconds of simulated time in the "normal" state, intra-GPe inhibitory connections and striatal inhibition were instantaneously switched to the "parkinsonian" state. This means that at $t = 5000\, ms$ the constant striatal current I_{app}^{GPe} applied into each GPe cell was switched from $-0.5\, \frac{pA}{(\mu m)^2}$ ("normal") to $-2.3\, \frac{pA}{(\mu m)^2}$ ("parkinsonian") and intra-GPe synaptic conductance $g_{GPe \to GPe}$ was switched from $1\, \frac{nS}{(\mu m)^2}$ ("normal") to $0\, \frac{nS}{(\mu m)^2}$ ("parkinsonian"). After other five seconds of simulation in the "parkinsonian" state, HFS of STN was turned

on at $t = 10000\,ms$. With the purpose of getting rid of transient phenomena, in quantifying the effectiveness of HFS in restoring thalamic responsiveness to sensorimotor input, we used only the simulation results of the last five seconds of a total of ten seconds of HFS simulation (from $t = 15000\,ms$ to $t = 20000\,ms$).

We used another periodic smoothed square wave current to model sensorimotor input to each thalamic cell. Amplitude, period, and pulse duration of this signal were respectively (same values as reported by Rubin and Terman [1]): $I_{SM}^{Thl} = 8\,\frac{pA}{(\mu m)^2}$, $T_{SM}^{Thl} = 50\,ms$ (which corresponds to $20\,Hz$ frequency) and $w_{SM}^{Thl} = 5\,ms$.

Two performance scores were used to evaluate HFS effectiveness: an *error index* (EI) and a *coeficient of variation* (CV). The EI is defined, as in Rubin and Terman (2004) [1], as the total number of errors divided by the total number of input stimuli. Two types of errors are counted: false positives and misses. False positives consist of multiple spikes after the most recent stimulus pulse. Misses are failures to respond within $10\,ms$ of the falling edge of the most recent stimulus pulse. A band of $\pm\,1mV$ arround a threshold of $-35\,mV$ was used to define a thalamic cell spike response. If the thalamic cell membrane voltage crossed first up and then down this band, we assumed that a spike response had occurred. The CV is defined, as in Grill et al. (2004) [9], as the standard deviation of the interspike time intervals divided by their mean. This coefficient is proposed, by Grill et al. [9], as a measure of variability and information content of the output of a thalamocortical cell. For the calculation of the CV we used the same band of $\pm\,1mV$ arround the threshold of $-35\,mV$ to define a thalamic cell spike response. Each performance score was calculated for the two thalamic cells of the model and the average over both cells was taken as the performance score associated to the corresponding stimulation parameters. Although EI and CV have been proposed as performance scores to measure thalamocortical cell responsiveness, we must be aware that by definition they can significantly differ on the performance evaluation.

When performing these simulations we found that for several combinations of stimulation parameters, STN firing was not strong enough to drive GPi cells and GPi remained silent with the consequence that thalamus was not inhibited at all. Of course this last picture is not coherent with Rubin and Terman's proposed mechanism for HFS action, which implies *tonic* firing of GPi. Suspecting that this was related to the way in which STN to GPi synaptical connections were programed, we modified the provided file in order to model these synapeses in the same way as reported by Rubin and Terman in [1] (i.e. with their own synaptical dynamics). With this modification, GPi fired for all combinations of stimulation parameters; so we finally adopted the modified file for our simulations. Original and modified versions of these synaptical connections are detailed in the appendix.

Results are plotted in figure 2. $EI = 0$ corresponds to one single spike response to each stimulus pulse withing $10\,ms$ of the falling edge of the stimulus pulse; $CV = 0$ corresponds to constant interspike time intervals. Both $EI = 0$ and $CV = 0$ are expected for a perfect relay of a periodic input, but of course $EI = 0$ is not incompatible with $CV \neq 0$ (for example if pulses are relayed but timing is slightly affected) and $CV = 0$ is not incompatible with $EI \neq 0$ (for example if one stimulus pulse is relayed periodically every two or more input pulses). For the parkinsonian unstimulated case (i.e. $I_{HFS}^{STN} = 0$), $EI = 0.54$ and $CV = 0.93$.

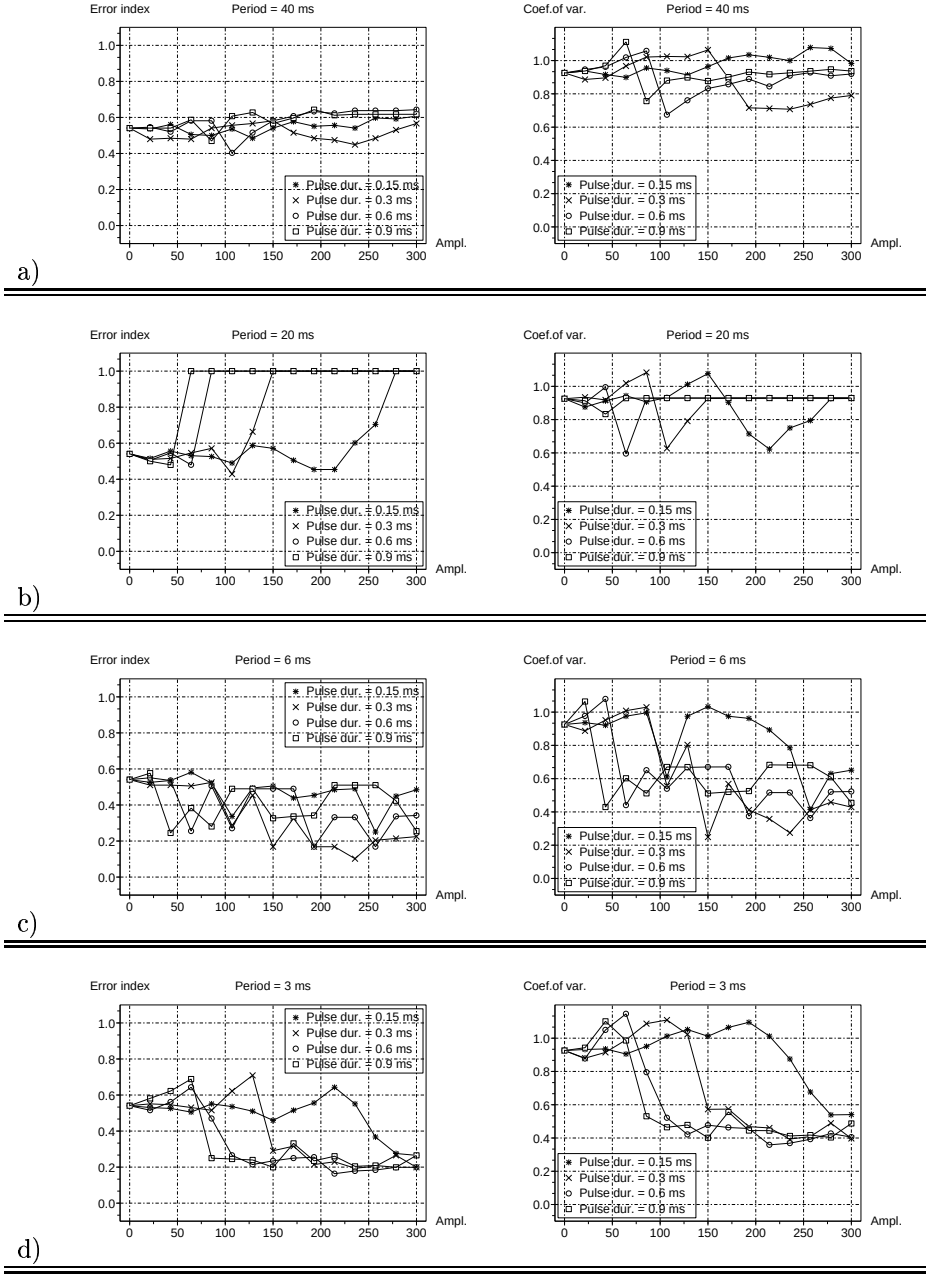

Figure 2: Error index (EI) (left column) and coeficient of variation (CV) (right column) dependence on HFS parameters. Each row corresponds to a different HFS period: a) $40\,ms$ ($25\,Hz$); b) $20\,ms$ ($50Hz$); c) $6\,ms$ ($167\,Hz$); d) $3\,ms$ ($333\,Hz$). Each plot contains different traces, one for each HFS pulse duration: $*$) $0.15\,ms$; $\times$) $0.3\,ms$; $\circ$) $0.6\,ms$; $\square$) $0.9\,ms$. Traces consist of interpolated performance socres against stimulation amplitude in $\frac{pA}{(\mu m)^2}$.

Regarding just the EI dependence on stimulation parameters, we observe that for a stimulation period of $20\,ms$ ($f_{HFS}^{STN} = 50\,Hz$), HFS actually worsens thalamic relay capability with respect to the unstimulated case for almost all stimulation amplitudes and pulse durations. This is in qualitative accordance with Rubin and Terman's observation that at "low" stimulation frequencies parkinsonian-like STN and GPe bursts still occur, but they become longer, leading to prolonged phases of strong inhibition from GPi to thalamocortical relay cells. As the stimulation period decreases (i.e. frequency increases), certain improvement is attained for a range of stimulation amplitudes and pulse durations, but this improvement is not as impressive as is tremor reduction in clinical experimentations. This is also the case for Rubin and Terman's reported results. Finally, for a stimulation period of $3\,ms$ ($f_{HFS}^{STN} = 333\,Hz$), we observe that improvement with respect to the parkinsonian unstimulated case is achieved at lower stimulation amplitudes as pulse duration is increased. This is also in qualitative agreement with Rubin and Terman's results.

The CV dependence on stimulation parameters follows a similar tendency to decrease with stimulation frequency for a range of stimulation amplitudes and pulse durations, but similarities with the EI dependence can not be taken too further.

We could reproduce Rubin and Terman's results *qualitatively* but not *quantitatively*. Several differences may contribute to this impossibility. In addition to the already mentioned differences in the number of cells included in each structure and the missing GPe to GPi connections, we can mention the following: 1) to compute the EI, we used the last $5\,s$ of simulated time (instead of a $1\,s$ interval as in [1]) 2) we discarded the first $5\,s$ of HFS simulated application with the intention of avoiding the effect of transient phenomena (a similar procedure was not reported by Rubin and Terman [1]) 3) the criteria we used for defining a thalamic cell spike response may be different from that used by Rubin and Terman (not reported).

Certainly the large amount of details necessary to completely specify the model is a source of reproducibility difficulties and is one of the costs associated with a fine detailed biologically realistic model.

4 Robustness

Rubin and Terman studied the robustness (section 3.4 in [1]) of the differential thalamocortical cells responsiveness to sensorimotor stimulation under "normal", "parkinsonian" and "parkinsonian with HFS of STN" conditions, with respect to noise in the sensorimotor input time course. They found that for the three conditions, the model is robust to random time intervals selected from both a uniform distribution and a Poisson distribution.

We next consider a simple parameter perturbation example to illustrate the sensitivity of thalamic capability to relay a periodic depolarizing input (quantified by an error index (EI) defined as in section 3), with respect to a pair of thalamic cell model parameters.

First, we took a set of HFS parameters ($I_{HFS}^{STN} = 150\,\frac{pA}{(\mu m)^2}$, $T_{HFS}^{STN} = 6\,ms$ and $w_{HFS}^{STN} = 0.3\,ms$) that achieves an error index of $EI = 0.16$ (average over the two thalamic cells) in the thalamic capability to relay a periodic smoothed square wave excitatory input current

($I_{SM}^{Thl} = 8\,\frac{pA}{(\mu m)^2}$, $T_{SM}^{Thl} = 50\,ms$ and $w_{SM}^{Thl} = 5\,ms$) in the "parkinsonian with HFS of STN" condition. Then, we simulated the full model for exactly the same conditions except for the fact that two parameters of the model were modified by 5%. For the perturbation example we perturbed parameters θ_r^{Thl} and $\sigma_{r\tau}^{Thl}$ (as defined in the appendix) by a 5% each. Simulation methodology was the same as described in section 3.

In table 1 we show the computed EI for each of the two thalamic cells of the model (EI_1 and EI_2) and the average thalamic error index (EI) for the unperturbed and perturbed case. Note that one of the thalamic cells switches from perfect relay function (i.e. $EI = 0$) to completely unfaithful responsiveness (i.e. $EI = 1$).

	Unperturbed $\theta_r^{Thl} = -84$ $\sigma_{r\tau}^{Thl} = 10.5$	Perturbed $\theta_r^{Thl} = -79.8$ $\sigma_{r\tau}^{Thl} = 11.025$
EI_1	0.34	0.74
EI_2	0	1
$EI = \frac{EI_1+EI_2}{2}$	0.17	0.87

Table 1: Sensitivity of thalamic capability to relay a periodic depolarizing input with respect to a particular parameter perturbation that affects two parameters of the thalamic cell model. EI_1 and EI_2 are the error indexes of the two thalamic cells of the full model and EI is the average between the former two and the associated index to the thalamus relay capability.

5 T-type Ca^{2+} current

Rubin and Terman [1] provided insight into the HFS mechanism underlying their simulation results. Analyzing their thalamic cell model (both in its full and reduced forms), with phase plane techniques, time scales separation and bifurcation diagrams; they show the prominent role of the low-threshold T-type Ca^{2+} current in affecting the thalamic cell responsiveness to depolarizing input pulses, under different patterns of thalamic inhibition from GPi: "normal", "parkinsonian" or "parkinsonian with HFS of STN". From this analysis, for the "parkinsonian" case it turns out that:

- As soon as an inhibition phase starts, the thalamic cell cannot fire in response to depolarizing input pulses until its T-current is sufficiently deinactivated. The slow building up of the available T-current is a cause of the new sustained higher inhibition level.
- As soon as it is released from an inhibition phase, the thalamic cell has an excess of T-current that (coupled with sodium deinactivation) leads to a burst response that

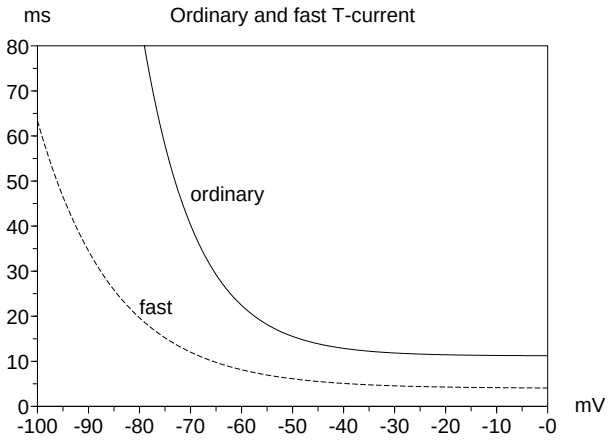

Figure 3: Effective "time constant" $\frac{\tau_r^{Thl}(v_M^{Thl})}{\phi_r^{Thl}}$ in ms against thalamic cell membrane voltage v_M^{Thl} in mV for the "ordinary" (continuous) and the "fast" (dashed) T-current.

interferes with the (normal) single spike response to each depolarizing input pulse. The burst extinguishes when the T-current is sufficiently inactivated.

Thus the T-current (increasing during an inhibitory phase and decreasing after an inhibitory phase) behaves as a compensatory system that allows the thalamic cell to respond even under phases of BG inhibition. The problem arises when these phases of inhibition appear periodically (with a period similar to the time it takes for the compensatory system to accommodate to the new situation). This causes lack of responsiveness at the onset of the inhibition phase and bursting after the end of the inhibition phase. This is why Rubin and Terman suggest that faster T-current inactivation and faster T-current deinactivation should improve thalamic cell responsiveness to depolarizing inputs even under "parkinsonian" inhibition from GPi.

To test these observations on the full computational model we performed simulations with two kinds of T-currents. An "ordinary" one, and a "fast" one obtained from the "ordinary" one by changing two parameters of the voltage-dependant "time constant" of the inactivation variable.

For the "ordinary" T-current we took all parameter values as specified in Terman's file. To simulate a "fast" T-current we decreased τ_{r0}^{Thl} and increased $\sigma_{r\tau}^{Thl}$ (see the appendix for the definition of these parameters). In figure 3 the voltage-dependent effective "time constant" $\frac{\tau_r^{Thl}(v_M^{Thl})}{\phi_r^{Thl}}$ (where $\phi_r = 2.5$) of the T-current inactivation variable r is shown for the "ordinary" and "fast" cases.

We set intra-GPe inhibitory connections ($g_{GPe\rightarrow GPe}$) and striatal inhibition to GPe (I_{app}^{GPe}) so as to simulate a "parkinsonian" state in which the STN-GPe peacemaker generates rhythmic tremor-like clustered activity. Under this "parkinsonian" state, we studied the effect

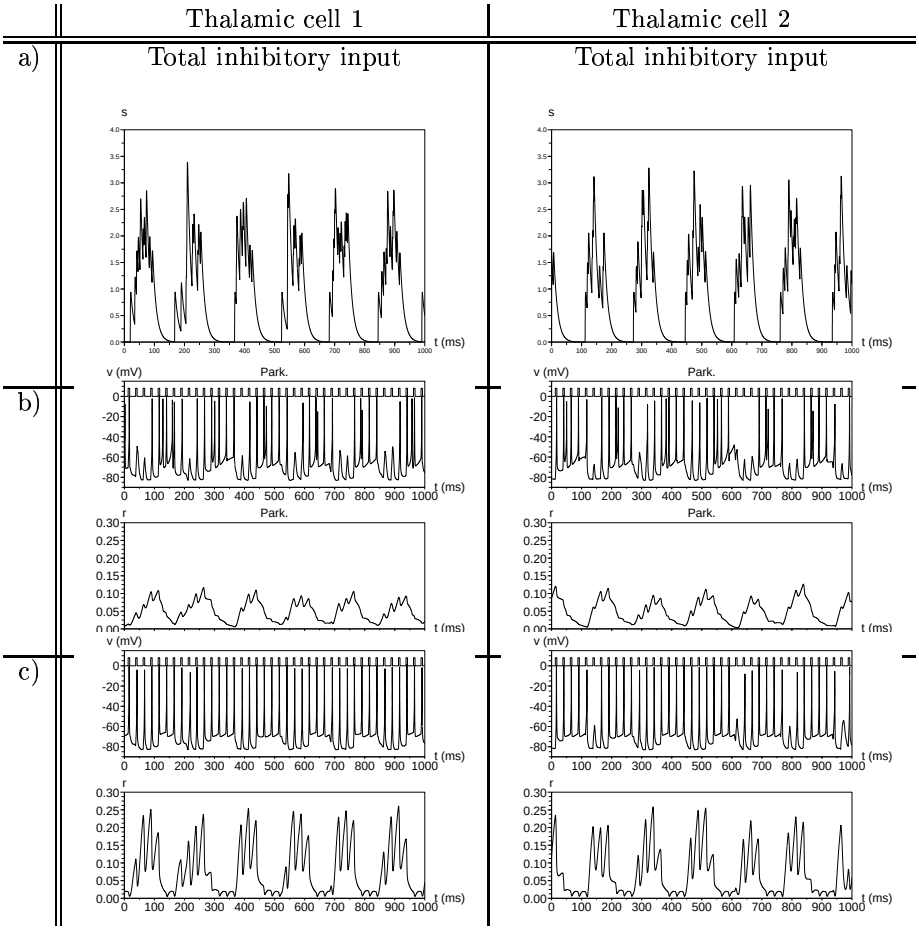

Figure 4: a) Total inhibitory synaptic input from GPi to each thalamic cell in the parkinsonian case. The almost periodic phases of inhibition occur at "tremor" frequency ($\approx 6.Hz$). b) and c) thalamic cells' responsiveness to an excitatory periodic signal for the "ordinary" and "fast" T-current cases respectively, under the same "parkinsonian" inhibition represented in a). For each of the two conditions represented in rows b) and c) two subfigures are reproduced for each cell: one with the thalamic cell membrane voltage in mV (lower trace) in response to the excitatory periodic current in $\frac{pA}{(\mu m)^2}$ (upper trace) and a lower subfigure with the corresponding evolution of the thalamic cell deinactivation variable r. Time axis has been shifted for clarity; $t = 0$ in the figure corresponds to $t = 19000\,ms$ in the simulated time course.

on the thalamic cell's responsiveness, of changing the "ordinary" T-current by the "fast" one, as previously defined.

In figure 4 we reproduce $1\,s$ of simulated thalamic cells's responses to excitatory periodic pulses, under "parkinsonian" inhibition from GPi, for the two different cases. For the "fast" T-current case, the deinactivation variable r reaches higher levels than in the the "ordinary" case, but transitions beetwen low and high levels of deinactivation are faster than in the "ordinary" case (note the sharper edges in the r time course). In table 2 we report the error indexes for the two different cases. From this table, it is clear that speeding up the T-current dynamics improves the responsiveness of the thalamic cell. This suggests that a chemically induced speeding up of T-current dynamics in thalamocortical relay cells, may provide an alternative treatment of parkinsonian motor disorders if Rubin and Terman's model is essentially valid. We do not know if this selective speeding up of a ion current is possible in practice. If it is possible, further experimentation in this direction could serve to develop a new drug-based therapeutic strategy. In any case, it could be a way of validating the proposed mechanism for HFS action.

	"Ordinary" T-current $\tau_{r0}^{Thl} = 28\,ms$ $\sigma_{r\tau}^{Thl} = 10.5\,mV$	"Fast" T-current $\tau_{r0}^{Thl} = 5\,ms$ $\sigma_{r\tau}^{Thl} = 15\,mV$
EI_1	0.36	0.030
EI_2	0.39	0.080
$EI = \frac{EI_1+EI_2}{2}$	0.37	0.055

Table 2: Thalamic capability to relay a periodic depolarizing input with an "ordinary" or a "fast" T-current. EI_1 and EI_2 are the error indexes of the two thalamic cells of the full model and EI is the average between the former two and the associated index to the thalamus relay capability. Only $1s$ of simulation is reproduced in figure 4, but the error indexes were calculated with $5\,s$ of simulated time (from $t = 15000\,ms$ to $t = 20000\,ms$)

6 The thalamic cell model

Following Rubin and Terman's analysis it turns out that, two key points account for the explanation of the proposed HFS mechanism: 1) The *pattern* of activity (either *phasic* or *tonic*) that sums up over all inhibitory afferents of a thalamocortical cell and 2) the intrinsic properties of the low-threshold T-type Ca^{2+} current of the same cell. If the pattern of inhibition is *phasic*, then the cell is seriously disrupted to relay the pulses that reach its excitatory input. But if the pattern of inhibition is *tonic*, then the cell is able to relay the excitatory pulses.

In order to explore this, we performed simulations with the isolated thalamic cell model. A prescribed time-dependent total inhibitory synaptic input $s(t)$ to the thalamic cell was

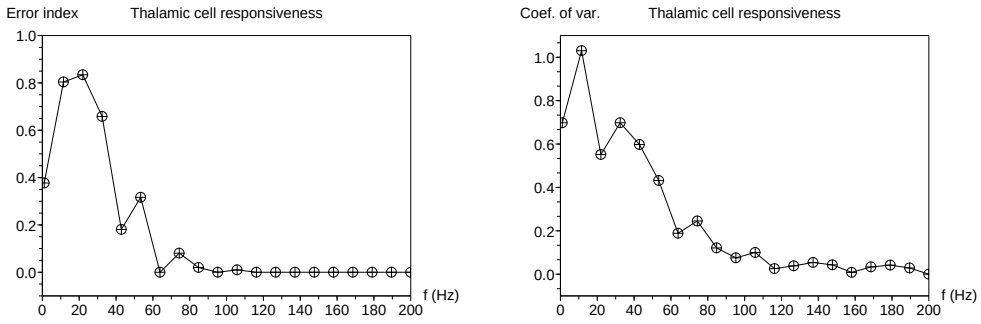

Figure 5: Error index (EI) (left) and coefficient of variation (CV) (right) associated to the thalamic cell model responsiveness capability, for different frequencies of the the inhibitory signal. Pulse duration of the inhibitory signal was always equal to half of the period. Performance scores were computed using the last $5\,s$ of a simulation time interval of $10\,s$.

used to model GPi inputs. We studied de dependence of the thalamic cell responsiveness on the fundamental frequency of $s(t)$.

We prescribed $s(t)$ to have a periodic smoothed square wave form:

$$s(t) = S\,Y\left(\sin\left(2\pi f_{inh}(t - d_{inh})\right)\right)\left(1 - Y\left(\sin\left(2\pi f_{inh}\left(t - d_{inh} + w_{inh}\right)\right)\right)\right)$$

where the sigmoidal function $Y(\cdot)$ has the form $Y(\cdot) = \left(1 + \exp\left(-\frac{\cdot}{\sigma_Y}\right)\right)^{-1}$ with $\sigma_Y = 0.001$. The amplitude $S = 2.5$ was selected according to the usual values observed in the simulations carried out with the complete model (see figure 4a to compare amplitudes of $s(t)$). Time shift $d_{inh} = -90\,ms$ was selected arbitrarily. The fundamental frequency f_{inh} of $s(t)$ was varied selecting values from a linearly spaced set of frequencies between $1\,Hz$ and $200\,Hz$ in order to emulate GPi firing in the "parkinsonian" ("low" frequency) and "HFS-driven" ("high" frequency) states. Pulse durations where selected equal to half the period: $w_{inh} = \frac{1}{2f_{inh}}$.

The periodic excitatory input current was kept unchanged with the form:

$$i_{exc}(t) = I_{exc}\,Y\left(\sin\left(2\pi f_{exc}(t - d_{exc})\right)\right)\left(1 - Y\left(\sin\left(2\pi f_{exc}\left(t - d_{exc} + w_{exc}\right)\right)\right)\right)$$

where $I_{exc} = 8\,\frac{pA}{(\mu m)^2}$, $T_{exc} = 25\,ms$ (which corresponds to $40\,Hz$ frequency), $w_{exc} = 5\,ms$, $d_{exc} = 80\,ms$ and $Y(\cdot)$ is the same sigmoidal function already used.

The error index (EI) and coeficient of variation (CV) associated to the thalamic cell responsiveness to its excitatory periodic input was calculated as explained in section 3. Fig-

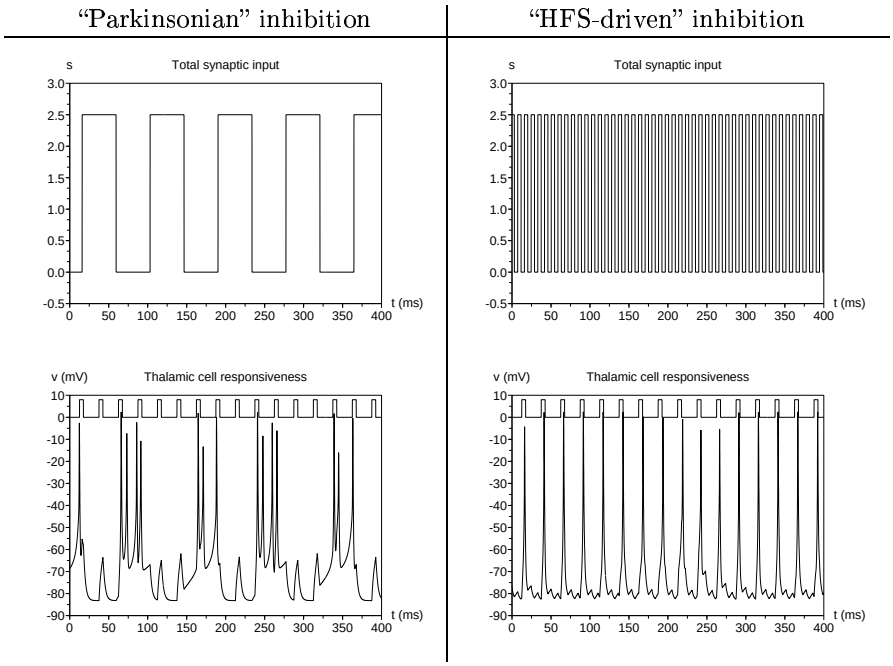

Figure 6: "Low" (left) and "high" (right) frequency prescribed inhibition signal $s(t)$ applied to the thalamic cell model and the corresponding thalamic cell responsiveness to the same excitatory input current (plotted in $\frac{pA}{(\mu m)^2}$ in the same subfigure as the membrane voltage v for comparison porpoises). Fundamental frequencies of $s(t)$ for the "low" and "high" frequency cases are $11.5\,Hz$ and $116\,Hz$ respectively. Time axis has been shifted for clarity, $t = 0$ in the figure corresponds to $t = 8000\,ms$.

ure 5 shows the EI and the CV against the fundamental frequency of $s(t)$ (f_{inh}). From these figures it is clear that "high" firing rates into the inhibitory input of the thalamic cell model are not contradictory with optimal relay of excitatory incoming pulses. Indeed these "high" firing rates excite the thalamic cell model dynamics in such a "fast" way that the T-current deinactivation remains almost constant. On the contrary, when the thalamic cell model is inhibited by a "low" frequency "parkinsonian-like" signal, the T-current deinactivation fluctuates trying to catch up with this "slow" inhibitory signal and the responsiveness to excitatory pulses is compromised. Two representative simulation results are reproduced in figure 6.

These results confirm Rubin and Terman's main result: *tonic* firing of GPi at high frequency can restore the ability of the thalamus to relay its sensorimotor input faithfully.

Moreover Rubin and Terman's explanation for HFS action, poses an interesting mathematical problem that could deserve deeper analysis if their explanation turns out to be physiologically valid: study of the synchronization of an excitable system (the Hodgkin-Huxley-like thalamic cell model) to an excitatory signal, under the inhibitory influence of patterned (i.e. "parkinsonian" or "HFS-driven") interference.

7 Conclusion

We examined some few aspects of the model by Rubin and Terman. The model relies on the physiological hypothesis that the main function of thalamus is to relay sensorimotor excitatory signals faithfully, even under the inhibitory influence of GPi activity.

Performing numerical simulations of the model dynamics we confirmed the claim that high firing rates in the output nucleus of the BG caused by HFS, *is not* contradictory with restoring thalamic relay function. Nevertheless, the beneficial effects of HFS measured by two performance scores (EI and CV), turned out to be much more clear in the simulation case of a an isolated thalamic cell with a prescribed inhibitory input signal (section 6) than in the full model simulation case (section 3). Clinically, it is well known that HFS efficiency in alleviating parkinsonian tremor, is strongly dependent on the stimulation frequency. This clear dependence was only observable in the isolated thalamic cell simulation results. Moreover we found that minor parameter perturbations can dramatically affect HFS efficiency in restoring thalamic relay function (section 4). This, suggests that although the full model provides a valuable qualitative explanation for HFS action, it still needs validation and adjustment against experimental data if it is supposed to be used as a predictive tool.

Focusing on the essential mechanisms that underlie HFS action in the proposed model we found, as pointed out by Rubin and Terman, that the T-current dynamical properties express in each thalamic cell in such a way that low frequency ("parkinsonian") inhibitory input signals are allowed to interfere with the normal relay function, while high frequency ("HFS driven") inhibitory input signals are prevented from interfering on normal relay function (see figure 5). Hence, in the model context, the basic action of HFS is to set a pattern of activity in GPi that is above the frequency domain of response of the thalamic cell T-current dynamics. This non-linear filtering effect poses an interesting mathematical problem

that deserves deeper investigation: study of the synchronization of an excitable system (the Huxley-like thalamic cell model) to an excitatory signal, under the inhibitory influence of patterned (i.e. "parkinsonian" or "HFS driven") interference.

Based on the insight provided by Rubin and Terman's explanation for HFS action, we experimented numerically with an attractive possibility that could become an alternative treatment to HFS if practicable. That is to speed up the T-current dynamics in order to make use of its compensatory effect against phases of inhibition (section 5). If the T-current deinactivation can follow the phases of inhibition sufficiently fast, the thalamic cell hyperpolarizes with each inhibition phase, but is still able to respond to excitatory stimuli even under this inhibitory phases because its T-current is sufficiently deinactivated (see figure 4). In this alternative, the frequency domain of response of the thalamic cell T-current dynamics is widened in order to follow the "parkinsonian" phases of inhibition.

Thus, in the context of the proposed model, the parkinsonian motor dysfunction arises when the the main frequency of inhibition to a thalamic cell is comparable to the characteristic "cut-off" frequency of its T-current dynamics. Separation of these frequencies may be achieved by two alternative ways: increasing the frequency of inhibition much higher above the cut-off frequency of the T-current dynamics (this is HFS), or increasing the "cut-off" frequency of the T-current dynamics in order to allow T-current deinactivation to follow quickly the "parkinsonian" phases of inhibition (this is speeding up the T-current dynamics).

A Details of Rubin and Terman's model

In this appendix we describe the mathematical model extracted from an XPPAUT file provided by David Terman. Each cell type is modeled with a single-compartment conductance-based biophysical Hodgkin-Huxley-like model. Every modification we made to the original file in order to perform our own simulations is indicated explicitely.

A.1 Differential equations associated to each cell model

For clarity, dependences of ion currents on membrane voltage and gating variables are omitted. See subsection A.2 of this appendix for the details of these dependences.

A.1.1 Differential equations for STN cells

$\forall j \in \{1,\ldots,8\}$:

$$\frac{d}{dt}v_M^{STN,j} = \frac{-i_L^{STN,j} - i_{Na}^{STN,j} - i_K^{STN,j} - i_{AHP}^{STN,j} - i_{Ca}^{STN,j} - i_T^{STN,j} - i_{GPe\to STN}^{STN,j} + jI_0^{STN} + i_{HFS}^{STN,j}}{C_M^{STN}}$$

$$\frac{d}{dt}h^{STN,j} = \phi_h^{STN}\frac{h_\infty^{STN}\left(v_M^{STN,j}\right) - h^{STN,j}}{\tau_h^{STN}\left(v_M^{STN,j}\right)}$$

$$\frac{d}{dt}n^{STN,j} = \phi_n^{STN}\frac{n_\infty^{STN}\left(v_M^{STN,j}\right) - n^{STN,j}}{\tau_n^{STN}\left(v_M^{STN,j}\right)}$$

$$\frac{d}{dt}r^{STN,j} = \phi_r^{STN}\frac{r_\infty^{STN}\left(v_M^{STN,j}\right) - r^{STN,j}}{\tau_r^{STN}\left(v_M^{STN,j}\right)}$$

$$\frac{d}{dt}x_{Ca}^{STN,j} = \phi_{x_{Ca}}^{STN}\epsilon_{x_{Ca}}^{STN}\left(-i_{Ca}^{STN,j} - i_T^{STN,j} - k_{Ca}^{STN}x_{Ca}^{STN,j}\right)$$
$$\frac{d}{dt}s^{STN,j} = \alpha^{STN}\left(1-s^{STN,j}\right)H_\infty^{STN}\left(v_M^{STN,j} - \theta_g^{STN}\right) - \beta^{STN}s^{STN,j}$$

A.1.2 Differential equations for GPe cells

$\forall j \in \{1,\ldots,8\}$:

$$\frac{d}{dt}v_M^{GPe,j} = \frac{-i_L^{GPe,j} - i_{Na}^{GPe,j} - i_K^{GPe,j} - i_{AHP}^{GPe,j} - i_{Ca}^{GPe,j} - i_T^{GPe,j} - i_{GPe\to GPe}^{GPe,j} - i_{STN\to GPe}^{GPe,j} + jI_0^{GPe} + I_{app}^{GPe}}{C_M^{GP}}$$
$$\frac{d}{dt}h^{GPe,j} = \phi_h^{GP}\frac{h_\infty^{GP}\left(v_M^{GPe,j}\right) - h^{GPe,j}}{\tau_h^{GP}\left(v_M^{GPe,j}\right)}$$
$$\frac{d}{dt}n^{GPe,j} = \phi_n^{GP}\frac{n_\infty^{GP}\left(v_M^{GPe,j}\right) - n^{GPe,j}}{\tau_n^{GP}\left(v_M^{GPe,j}\right)}$$
$$\frac{d}{dt}r^{GPe,j} = \phi_r^{GP}\frac{r_\infty^{GP}\left(v_M^{GPe,j}\right) - r^{GPe,j}}{\tau_r^{GP}}$$
$$\frac{d}{dt}x_{Ca}^{GPe,j} = \epsilon_{x_{Ca}}^{GP}\left(-i_{Ca}^{GPe,j} - i_T^{GPe,j} - k_{Ca}^{GP}x_{Ca}^{GPe,j}\right)$$
$$\frac{d}{dt}s^{GPe,j} = \alpha^{GP}\left(1-s^{GPe,j}\right)H_\infty^{GP}\left(v_M^{GPe,j} - \theta_g^{GP}\right) - \beta^{GPe}s^{GPe,j}$$

A.1.3 Differential equations for GPi cells

$\forall j \in \{1,\ldots,8\}$:

$$\frac{d}{dt}v_M^{GPi,j} = \frac{-i_L^{GPi,j} - i_{Na}^{GPi,j} - i_K^{GPi,j} - i_{AHP}^{GPi,j} - i_{Ca}^{GPi,j} - i_T^{GPi,j} - i_{STN\to GPi}^{GPi,j} + I_{app}^{GPi}}{C_M^{GP}}$$
$$\frac{d}{dt}h^{GPi,j} = \phi_h^{GP}\frac{h_\infty^{GP}\left(v_M^{GPi,j}\right) - h^{GPi,j}}{\tau_h^{GP}\left(v_M^{GPi,j}\right)}$$
$$\frac{d}{dt}n^{GPi,j} = \phi_n^{GP}\frac{n_\infty^{GP}\left(v_M^{GPi,j}\right) - n^{GPi,j}}{\tau_n^{GP}\left(v_M^{GPi,j}\right)}$$
$$\frac{d}{dt}r^{GPi,j} = \phi_r^{GP}\frac{r_\infty^{GP}\left(v_M^{GPi,j}\right) - r^{GPi,j}}{\tau_r^{GP}}$$
$$\frac{d}{dt}x_{Ca}^{GPi,j} = \epsilon_{x_{Ca}}^{GP}\left(-i_{Ca}^{GPi,j} - i_T^{GPi,j} - k_{Ca}^{GP}x_{Ca}^{GPi,j}\right)$$
$$\frac{d}{dt}s^{GPi,j} = \alpha^{GP}\left(1-s^{GPi,j}\right)H_\infty^{GP}\left(v_M^{GPi,j} - \theta_g^{GP}\right) - \beta^{GPi}s^{GPi,j}$$

A.1.4 Differential equations for thalamic cells

$\forall j \in \{1,2\}$:

$$\frac{d}{dt}v_M^{Thl,j} = \frac{-i_L^{Thl,j} - i_{Na}^{Thl,j} - i_K^{Thl,j} - i_T^{Thl,j} - i_{GPi\to Thl}^{Thl,j} + i_{SM}^{Thl,j}}{C_M^{Thl}}$$
$$\frac{d}{dt}h^{Thl,j} = \phi_h^{Thl}\frac{h_\infty^{Thl}\left(v_M^{Thl,j}\right) - h^{Thl,j}}{\tau_h^{Thl}\left(v_M^{Thl,j}\right)}$$
$$\frac{d}{dt}r^{Thl,j} = \phi_r^{Thl}\frac{r_\infty^{Thl}\left(v_M^{Thl,j}\right) - r^{Thl,j}}{\tau_r^{Thl}\left(v_M^{Thl,j}\right)}$$

A.2 Ion currents

A.2.1 STN cells' currents

$\forall j \in \{1,\dots,8\}$:

$$i_L^{STN,j} = g_L^{STN}\left(v_M^{STN,j} - V_L^{STN}\right)$$
$$i_{Na}^{STN,j} = g_{Na}^{STN}\left(m_\infty^{STN}\left(v_M^{STN,j}\right)\right)^3 h^{STN,j}\left(v_M^{STN,j} - V_{Na}^{STN}\right)$$
$$i_K^{STN,j} = g_K^{STN}\left(n^{STN,j}\right)^4\left(v_M^{STN,j} - V_K^{STN}\right)$$
$$i_{AHP}^{STN,j} = g_{AHP}^{STN}\left(v_M^{STN,j} - V_K^{STN}\right)\frac{x_{Ca}^{STN,j}}{x_{Ca}^{STN,j}+k_1^{STN}}$$
$$i_{Ca}^{STN,j} = g_{Ca}^{STN}\left(s_\infty^{STN}\left(v_M^{STN,j}\right)\right)^2\left(v_M^{STN,j} - V_{Ca}^{STN}\right)$$
$$i_T^{STN,j} = g_T^{STN}\left(a_\infty^{STN}\left(v_M^{STN,j}\right)\right)^3\left(b_\infty^{STN}\left(r^{STN,j}\right)\right)^2\left(v_M^{STN,j} - V_{Ca}^{STN}\right)$$
$$i_{GPe\to STN}^{STN,j} = g_{GPe\to STN}\left(v_M^{STN,j} - V_{GPe\to STN}\right)s_{GPe\to STN}^{STN,j}$$
$$i_{HFS}^{STN,j} = \begin{cases} I_{HFS}^{STN} Y\left(\sin\left(\omega_{HFS}^{STN} t\right) - a_{HFS}^{STN}\right) & \text{(Terman's file)} \\ I_{HFS}^{STN} Y\left(\sin\left(\frac{2\pi t}{T_{HFS}^{STN}}\right)\right)\left(1 - Y\left(\sin\left(\frac{2\pi\left(t+w_{HFS}^{STN}\right)}{T_{HFS}^{STN}}\right)\right)\right) & \text{(Our simulations)} \end{cases}$$

A.2.2 GPe cells' currents

$\forall j \in \{1,\dots,8\}$:

$$i_L^{GPe,j} = g_L^{GP}\left(v_M^{GPe,j} - V_L^{GP}\right)$$
$$i_{Na}^{GPe,j} = g_{Na}^{GP}\left(m_\infty^{GP}\left(v_M^{GPe,j}\right)\right)^3 h^{GPe,j}\left(v_M^{GPe,j} - V_{Na}^{GP}\right)$$
$$i_K^{GPe,j} = g_K^{GP}\left(n^{GPe,j}\right)^4\left(v_M^{GPe,j} - V_K^{GP}\right)$$
$$i_{AHP}^{GPe,j} = g_{AHP}^{GP}\left(v_M^{GPe,j} - V_K^{GP}\right)\frac{x_{Ca}^{GPe,j}}{x_{Ca}^{GPe,j}+k_1^{GP}}$$
$$i_{Ca}^{GPe,j} = g_{Ca}^{GP}\left(s_\infty^{GP}\left(v_M^{GPe,j}\right)\right)^2\left(v_M^{GPe,j} - V_{Ca}^{GP}\right)$$
$$i_T^{GPe,j} = g_T^{GP}\left(a_\infty^{GP}\left(v_M^{GPe,j}\right)\right)^3 r^{GPe,j}\left(v_M^{GPe,j} - V_{Ca}^{GP}\right)$$
$$i_{GPe\to GPe}^{GPe,j} = g_{GPe\to GPe}\left(v_M^{GPe,j} - V_{GPe\to GPe}\right)s_{GPe\to GPe}^{GPe,j}$$
$$i_{STN\to GPe}^{GPe,j} = g_{STN\to GPe}\left(v_M^{GPe,j} - V_{STN\to GPe}\right)s_{STN\to GPe}^{GPe,j}$$

A.2.3 GPi cells' currents

$\forall j \in \{1,\dots,8\}$:

$$i_L^{GPi,j} = g_L^{GP}\left(v_M^{GPi,j} - V_L^{GP}\right)$$

$$i_{Na}^{GPi,j} = g_{Na}^{GP}\left(m_{\infty}^{GP}\left(v_M^{GPi,j}\right)\right)^3 h^{GPi,j}\left(v_M^{GPi,j} - V_{Na}^{GP}\right)$$
$$i_{K}^{GPi,j} = g_{K}^{GP}\left(n^{GPi,j}\right)^4\left(v_M^{GPi,j} - V_{K}^{GP}\right)$$
$$i_{AHP}^{GPi,j} = g_{AHP}^{GP}\left(v_M^{GPi,j} - V_{K}^{GP}\right)\frac{x_{Ca}^{GPi,j}}{x_{Ca}^{GPi,j}+k_1^{GP}}$$
$$i_{Ca}^{GPi,j} = g_{Ca}^{GP}\left(s_{\infty}^{GP}\left(v_M^{GPi,j}\right)\right)^2\left(v_M^{GPi,j} - V_{Ca}^{GP}\right)$$
$$i_{T}^{GPi,j} = g_{T}^{GP}\left(a_{\infty}^{GP}\left(v_M^{GPi,j}\right)\right)^3 r^{GPi,j}\left(v_M^{GPi,j} - V_{Ca}^{GP}\right)$$
$$i_{STN\to GPi}^{GPi,j} = \begin{cases} g_{STN\to GPi}\left(v_M^{GPi,j} - V_{STN\to GPi}\right) Y\left(v_{STN\to GPi}^{GPi,j} - \theta_{STN\to GPi}\right) & \text{(Terman's file)} \\ g_{STN\to GPi}\left(v_M^{GPi,j} - V_{STN\to GPi}\right) s_{STN\to GPi}^{GPi,j} & \text{(Our simulations)} \end{cases}$$

A.2.4 Thalamic cells' currents

$\forall j \in \{1,2\}$:
$$i_{L}^{Thl,j} = g_{L}^{Thl}\left(v_M^{Thl,j} - V_{L}^{Thl}\right)$$
$$i_{Na}^{Thl,j} = g_{Na}^{Thl}\left(m_{\infty}^{Thl}\left(v_M^{Thl,j}\right)\right)^3 h^{Thl,j}\left(v_M^{Thl,j} - V_{Na}^{Thl}\right)$$
$$i_{K}^{Thl,j} = g_{K}^{Thl}\left(0.75\left(1-h^{Thl,j}\right)\right)^4\left(v_M^{Thl,j} - V_{K}^{Thl}\right)$$
$$i_{T}^{Thl,j} = g_{T}^{Thl}\left(p_{\infty}^{Thl}\left(v_M^{Thl,j}\right)\right)^2 r^{Thl,j}\left(v_M^{Thl,j} - V_{T}^{Thl}\right)$$
$$i_{GPi\to Thl}^{Thl,j} = g_{GPi\to Thl}\left(v_M^{Thl,j} - V_{GPi\to Thl}\right) s_{GPi\to Thl}^{Thl,j}$$
$$i_{SM}^{Thl,j} = I_{SM}^{Thl} Y\left(\sin\left(\frac{2\pi\left(t-d_{SM}^{Thl}\right)}{T_{SM}^{Thl}}\right)\right)\left(1 - Y\left(\sin\left(\frac{2\pi\left(t-d_{SM}^{Thl}+w_{SM}^{Thl}\right)}{T_{SM}^{Thl}}\right)\right)\right)$$

A.3 Gating functions

A.3.1 STN cells' gating functions

$$m_{\infty}^{STN}(\cdot) = \frac{1}{1+\exp\left(-\frac{\cdot-\theta_m^{STN}}{\sigma_m^{STN}}\right)}$$
$$h_{\infty}^{STN}(\cdot) = \frac{1}{1+\exp\left(\frac{\cdot-\theta_h^{STN}}{\sigma_h^{STN}}\right)}$$
$$n_{\infty}^{STN}(\cdot) = \frac{1}{1+\exp\left(-\frac{\cdot-\theta_n^{STN}}{\sigma_n^{STN}}\right)}$$
$$s_{\infty}^{STN}(\cdot) = \frac{1}{1+\exp\left(-\frac{\cdot-\theta_s^{STN}}{\sigma_s^{STN}}\right)}$$
$$a_{\infty}^{STN}(\cdot) = \frac{1}{1+\exp\left(-\frac{\cdot-\theta_a^{STN}}{\sigma_a^{STN}}\right)}$$
$$b_{\infty}^{STN}(\cdot) = \frac{1}{1+\exp\left(-\frac{\cdot-\theta_b^{STN}}{\sigma_b^{STN}}\right)} - \frac{1}{1+\exp\left(\frac{\theta_b^{STN}}{\sigma_b^{STN}}\right)}$$

$$r_{\infty}^{STN}(\cdot) = \frac{1}{1+\exp\left(\frac{\cdot-\theta_{r}^{STN}}{\sigma_{r}^{STN}}\right)}$$
$$\tau_{h}^{STN}(\cdot) = \tau_{h0}^{STN} + \frac{\tau_{h1}^{STN}}{1+\exp\left(\frac{\cdot-\theta_{h\tau}^{STN}}{\sigma_{h\tau}^{STN}}\right)}$$
$$\tau_{n}^{STN}(\cdot) = \tau_{n0}^{STN} + \frac{\tau_{n1}^{STN}}{1+\exp\left(\frac{\cdot-\theta_{n\tau}^{STN}}{\sigma_{n\tau}^{STN}}\right)}$$
$$\tau_{r}^{STN}(\cdot) = \tau_{r0}^{STN} + \frac{\tau_{r1}^{STN}}{1+\exp\left(\frac{\cdot-\theta_{r\tau}^{STN}}{\sigma_{r\tau}^{STN}}\right)}$$
$$H_{\infty}^{STN}(\cdot) = \frac{1}{1+\exp\left(-\frac{\cdot-\theta_{gH}^{STN}}{\sigma_{gH}^{STN}}\right)}$$

A.3.2 GPe and GPi cells' shared gating functions

$$m_{\infty}^{GP}(\cdot) = \frac{1}{1+\exp\left(-\frac{\cdot-\theta_{m}^{GP}}{\sigma_{m}^{GP}}\right)}$$
$$h_{\infty}^{GP}(\cdot) = \frac{1}{1+\exp\left(\frac{\cdot-\theta_{h}^{GP}}{\sigma_{h}^{GP}}\right)}$$
$$n_{\infty}^{GP}(\cdot) = \frac{1}{1+\exp\left(-\frac{\cdot-\theta_{n}^{GP}}{\sigma_{n}^{GP}}\right)}$$
$$s_{\infty}^{GP}(\cdot) = \frac{1}{1+\exp\left(-\frac{\cdot-\theta_{s}^{GP}}{\sigma_{s}^{GP}}\right)}$$
$$a_{\infty}^{GP}(\cdot) = \frac{1}{1+\exp\left(-\frac{\cdot-\theta_{a}^{GP}}{\sigma_{a}^{GP}}\right)}$$
$$r_{\infty}^{GP}(\cdot) = \frac{1}{1+\exp\left(\frac{\cdot-\theta_{r}^{GP}}{\sigma_{r}^{GP}}\right)}$$
$$\tau_{h}^{GP}(\cdot) = \tau_{h0}^{GP} + \frac{\tau_{h1}^{GP}}{1+\exp\left(\frac{\cdot-\theta_{h\tau}^{GP}}{\sigma_{h\tau}^{GP}}\right)}$$
$$\tau_{n}^{GP}(\cdot) = \tau_{n0}^{GP} + \frac{\tau_{n1}^{GP}}{1+\exp\left(\frac{\cdot-\theta_{n\tau}^{GP}}{\sigma_{n\tau}^{GP}}\right)}$$
$$H_{\infty}^{GP}(\cdot) = \frac{1}{1+\exp\left(-\frac{\cdot-\theta_{gH}^{GP}}{\sigma_{gH}^{GP}}\right)}$$

A.3.3 Thalamic cells' gating functions

$$m_{\infty}^{Thl}(\cdot) = \frac{1}{1+\exp\left(-\frac{\cdot-\theta_{m}^{Thl}}{\sigma_{m}^{Thl}}\right)}$$
$$h_{\infty}^{Thl}(\cdot) = \frac{1}{1+\exp\left(\frac{\cdot-\theta_{h}^{Thl}}{\sigma_{h}^{Thl}}\right)}$$
$$p_{\infty}^{Thl}(\cdot) = \frac{1}{1+\exp\left(-\frac{\cdot-\theta_{p}^{Thl}}{\sigma_{p}^{Thl}}\right)}$$

$$r_{\infty}^{Thl}(\cdot) = \frac{1}{1+\exp\left(\frac{\cdot-\theta_{r}^{Thl}}{\sigma_{r}^{Thl}}\right)}$$
$$a_{h}^{Thl}(\cdot) = a_{h0}^{Thl}\exp\left(-\frac{\cdot-\theta_{ah}^{Thl}}{\sigma_{ah}^{Thl}}\right)$$
$$b_{h}^{Thl}(\cdot) = \frac{b_{h0}^{Thl}}{1+\exp\left(-\frac{\cdot-\theta_{bh}^{Thl}}{\sigma_{bh}^{Thl}}\right)}$$
$$\tau_{h}^{Thl}(\cdot) = \frac{1}{a_{h}^{Thl}(\cdot)+b_{h}^{Thl}(\cdot)}$$
$$\tau_{r}^{Thl}(\cdot) = \tau_{r0}^{Thl} + \tau_{r1}^{Thl}\exp\left(-\frac{\cdot-\theta_{\tau r}^{Thl}}{\sigma_{\tau r}^{Thl}}\right)$$

A.3.4 Auxiliary sigmoidal function

$$Y(\cdot) = \frac{1}{1+\exp\left(-\frac{\cdot}{\sigma_{Y}}\right)}$$

A.4 Connections among cells

A.4.1 From GPe to STN

$$\begin{pmatrix} s_{GPe\rightarrow STN}^{STN,1} \\ s_{GPe\rightarrow STN}^{STN,2} \\ s_{GPe\rightarrow STN}^{STN,3} \\ s_{GPe\rightarrow STN}^{STN,4} \\ s_{GPe\rightarrow STN}^{STN,5} \\ s_{GPe\rightarrow STN}^{STN,6} \\ s_{GPe\rightarrow STN}^{STN,7} \\ s_{GPe\rightarrow STN}^{STN,8} \end{pmatrix} = \begin{pmatrix} 0 & 1 & 0 & 0 & 1 & 0 & 0 & 0 \\ 1 & 0 & 0 & 0 & 0 & 1 & 0 & 0 \\ 0 & 0 & 0 & 1 & 0 & 0 & 0 & 1 \\ 0 & 0 & 1 & 0 & 0 & 0 & 1 & 0 \\ 0 & 1 & 0 & 0 & 0 & 1 & 0 & 0 \\ 1 & 0 & 0 & 0 & 1 & 0 & 0 & 0 \\ 0 & 0 & 1 & 0 & 0 & 0 & 0 & 1 \\ 0 & 0 & 0 & 1 & 0 & 0 & 1 & 0 \end{pmatrix} \begin{pmatrix} s^{GPe,1} \\ s^{GPe,2} \\ s^{GPe,3} \\ s^{GPe,4} \\ s^{GPe,5} \\ s^{GPe,6} \\ s^{GPe,7} \\ s^{GPe,8} \end{pmatrix}$$

A.4.2 From GPe to GPe

$$\begin{pmatrix} s_{GPe\rightarrow GPe}^{GPe,1} \\ s_{GPe\rightarrow GPe}^{GPe,2} \\ s_{GPe\rightarrow GPe}^{GPe,3} \\ s_{GPe\rightarrow GPe}^{GPe,4} \\ s_{GPe\rightarrow GPe}^{GPe,5} \\ s_{GPe\rightarrow GPe}^{GPe,6} \\ s_{GPe\rightarrow GPe}^{GPe,7} \\ s_{GPe\rightarrow GPe}^{GPe,8} \end{pmatrix} = \begin{pmatrix} 0 & 1 & 1 & 0 & 0 & 0 & 0 & 0 \\ 1 & 0 & 0 & 0 & 1 & 0 & 0 & 0 \\ 0 & 0 & 0 & 1 & 0 & 0 & 0 & 1 \\ 1 & 0 & 1 & 0 & 0 & 0 & 0 & 0 \\ 0 & 0 & 0 & 0 & 0 & 1 & 1 & 0 \\ 0 & 1 & 0 & 0 & 1 & 0 & 0 & 0 \\ 0 & 0 & 1 & 0 & 0 & 0 & 0 & 1 \\ 0 & 0 & 0 & 1 & 0 & 0 & 1 & 0 \end{pmatrix} \begin{pmatrix} s^{GPe,1} \\ s^{GPe,2} \\ s^{GPe,3} \\ s^{GPe,4} \\ s^{GPe,5} \\ s^{GPe,6} \\ s^{GPe,7} \\ s^{GPe,8} \end{pmatrix}$$

A.4.3 From STN to GPe

$$\begin{pmatrix} s^{GPe,1}_{STN\to GPe} \\ s^{GPe,2}_{STN\to GPe} \\ s^{GPe,3}_{STN\to GPe} \\ s^{GPe,4}_{STN\to GPe} \\ s^{GPe,5}_{STN\to GPe} \\ s^{GPe,6}_{STN\to GPe} \\ s^{GPe,7}_{STN\to GPe} \\ s^{GPe,8}_{STN\to GPe} \end{pmatrix} = \begin{pmatrix} 0&0&0&1&0&0&0&1 \\ 0&0&1&0&0&0&1&0 \\ 1&0&0&0&1&0&0&0 \\ 0&1&0&0&0&1&0&0 \\ 0&0&0&1&0&0&0&1 \\ 0&0&1&0&0&0&1&0 \\ 0&1&0&0&1&0&0&0 \\ 1&0&0&0&0&1&0&0 \end{pmatrix} \begin{pmatrix} s^{STN,1} \\ s^{STN,2} \\ s^{STN,3} \\ s^{STN,4} \\ s^{STN,5} \\ s^{STN,6} \\ s^{STN,7} \\ s^{STN,8} \end{pmatrix}$$

A.4.4 From STN to GPi

$$\begin{pmatrix} v^{GPi,1}_{STN\to GPi} \\ v^{GPi,2}_{STN\to GPi} \\ v^{GPi,3}_{STN\to GPi} \\ v^{GPi,4}_{STN\to GPi} \\ v^{GPi,5}_{STN\to GPi} \\ v^{GPi,6}_{STN\to GPi} \\ v^{GPi,7}_{STN\to GPi} \\ v^{GPi,8}_{STN\to GPi} \end{pmatrix} = \begin{pmatrix} 1&0&0&0&0&0&0&0 \\ 0&1&0&0&0&0&0&0 \\ 0&0&1&0&0&0&0&0 \\ 0&0&0&1&0&0&0&0 \\ 0&0&0&0&1&0&0&0 \\ 0&0&0&0&0&1&0&0 \\ 0&0&0&0&0&0&1&0 \\ 0&0&0&0&0&0&0&1 \end{pmatrix} \begin{pmatrix} v^{STN,1}_{M} \\ v^{STN,2}_{M} \\ v^{STN,3}_{M} \\ v^{STN,4}_{M} \\ v^{STN,5}_{M} \\ v^{STN,6}_{M} \\ v^{STN,7}_{M} \\ v^{STN,8}_{M} \end{pmatrix}$$

(Terman's file)

$$\begin{pmatrix} s^{GPi,1}_{STN\to GPi} \\ s^{GPi,2}_{STN\to GPi} \\ s^{GPi,3}_{STN\to GPi} \\ s^{GPi,4}_{STN\to GPi} \\ s^{GPi,5}_{STN\to GPi} \\ s^{GPi,6}_{STN\to GPi} \\ s^{GPi,7}_{STN\to GPi} \\ s^{GPi,8}_{STN\to GPi} \end{pmatrix} =$$

$$\begin{pmatrix} 1&0&0&0&0&0&0&0 \\ 0&1&0&0&0&0&0&0 \\ 0&0&1&0&0&0&0&0 \\ 0&0&0&1&0&0&0&0 \\ 0&0&0&0&1&0&0&0 \\ 0&0&0&0&0&1&0&0 \\ 0&0&0&0&0&0&1&0 \\ 0&0&0&0&0&0&0&1 \end{pmatrix} \begin{pmatrix} s^{STN,1} \\ s^{STN,2} \\ s^{STN,3} \\ s^{STN,4} \\ s^{STN,5} \\ s^{STN,6} \\ s^{STN,7} \\ s^{STN,8} \end{pmatrix}$$

(Our simulations)

A.4.5 From GPi to Thl

$$\begin{pmatrix} s^{Thl,1}_{GPi\to Thl} \\ s^{Thl,2}_{GPi\to Thl} \end{pmatrix} = \begin{pmatrix} 1&1&0&0&1&1&0&0 \\ 0&0&1&1&0&0&1&1 \end{pmatrix} \begin{pmatrix} s^{GPi,1} \\ s^{GPi,2} \\ s^{GPi,3} \\ s^{GPi,4} \\ s^{GPi,5} \\ s^{GPi,6} \\ s^{GPi,7} \\ s^{GPi,8} \end{pmatrix}$$

A.5 Parameters

A.5.1 STN cells' parameters

- Membrane capacitance:

Parameter	Value
C_M^{STN}	$1\,\frac{pF}{(\mu m)^2}$

- Leak current related parameters:

Parameter	Value
g_L^{STN}	$2.25\,\frac{nS}{(\mu m)^2}$
V_L^{STN}	$-60\,mV$

- Sodium current related parameters:

Parameter	Value
g_{Na}^{STN}	$37.5\,\frac{nS}{(\mu m)^2}$
V_{Na}^{STN}	$55\,mV$
θ_m^{STN}	$-30\,mV$
σ_m^{STN}	$15\,mV$
θ_h^{STN}	$-39\,mV$
σ_h^{STN}	$3.1\,mV$
τ_{h0}^{STN}	$1\,ms$
τ_{h1}^{STN}	$500\,ms$
$\theta_{h\tau}^{STN}$	$-57\,mV$
$\sigma_{h\tau}^{STN}$	$3\,mV$
ϕ_h^{STN}	0.75

- Potasium current related parameters:

Parameter	Value
g_K^{STN}	$45\,\frac{nS}{(\mu m)^2}$
V_K^{STN}	$-80\,mV$
θ_n^{STN}	$-32\,mV$
σ_n^{STN}	$8\,mV$
τ_{n0}^{STN}	$1\,ms$
τ_{n1}^{STN}	$100\,ms$
$\theta_{n\tau}^{STN}$	$-80\,mV$
$\sigma_{n\tau}^{STN}$	$26\,mV$
ϕ_n^{STN}	0.75

- High-threshold calcium current related parameters:

Parameter	Value
g_{Ca}^{STN}	$0.5\,\frac{nS}{(\mu m)^2}$
V_{Ca}^{STN}	$140\,mV$
θ_s^{STN}	$-39\,mV$
σ_s^{STN}	$8\,mV$

- Low-threshold T-type calcium current related parameters:

Parameter	Value
g_T^{STN}	$0.5\,\frac{nS}{(\mu m)^2}$
θ_a^{STN}	$-63\,mV$
σ_a^{STN}	$7.8\,mV$
θ_b^{STN}	$0.25\,mV$
σ_b^{STN}	$0.07\,mV$
θ_r^{STN}	$-67\,mV$
σ_r^{STN}	$2\,mV$
τ_{r0}^{STN}	$7.1\,ms$
τ_{r1}^{STN}	$17.5\,ms$
$\theta_{r\tau}^{STN}$	$68\,mV$
$\sigma_{r\tau}^{STN}$	$2.2\,mV$
ϕ_r^{STN}	0.5

- Calcium-activated voltage-independent "afterhyperpolarization" potasium current related parameters:

Parameter	Value
g_{AHP}^{STN}	$9\,\frac{nS}{(\mu m)^2}$
k_1^{STN}	15
k_{Ca}^{STN}	$22.5\,\frac{pA}{(\mu m)^2}$
$\phi_{x_{Ca}}^{STN}$	0.75
$\epsilon_{x_{Ca}}^{STN}$	$5\times10^{-5}\,\frac{(\mu m)^2}{pA}(ms)^{-1}$

- Synaptic state-variables related parameters:

Parameter	Value
α^{STN}	5
β^{STN}	1
θ_g^{STN}	$30\,mV$
θ_{gH}^{STN}	$-39\,mV$
σ_{gH}^{STN}	$8\,mV$

- Afferent synaptic currents related parameters:

Parameter	Value
$g_{GPe \rightarrow STN}$	$0.9 \frac{nS}{(\mu m)^2}$
$V_{GPe \rightarrow STN}$	$-100\, mV$

- Constant current (used to multiply by the cell index number to create slight imbalance):

Parameter	Value
I_0^{STN}	$2 \frac{pA}{(\mu m)^2}$

- HFS related parameters (Terman's file):

Parameter	Value
I_{HFS}^{STN}	$0 \frac{pA}{(\mu m)^2}$ (no HFS) ; $400 \frac{pA}{(\mu m)^2}$ (HFS)
ω_{HFS}^{STN}	$0.5 \frac{rad}{ms}$
a_{HFS}^{STN}	0.9

- HFS related parameters (Our simulations):

Parameter	Value
I_{HFS}^{STN}	$0 \frac{pA}{(\mu m)^2}$ (no HFS) ; $21.43, 42.86, 64.29, 85.71, 107.1, 128.6, 150.0, 171.4, 192.9, 214.3, 235.7, 257.1, 278.6, 300.0 \frac{pA}{(\mu m)^2}$ (HFS)
T_{HFS}^{STN}	$3.00, 6.00, 20.0, 40.0 ms$
w_{HFS}^{STN}	$0.150, 0.300, 0.600, 0.900 ms$

A.5.2 GPe and GPi cells' shared parameters

- Membrane capacitance:

Parameter	Value
C_M^{GP}	$1 \frac{pF}{(\mu m)^2}$

- Leak current related parameters:

Parameter	Value
g_L^{GP}	$0.1 \frac{nS}{(\mu m)^2}$
V_L^{GP}	$-55\, mV$

- Sodium current related parameters:

Parameter	Value
g_{Na}^{GP}	$120\ \frac{nS}{(\mu m)^2}$
V_{Na}^{GP}	$55\,mV$
θ_m^{GP}	$-37\,mV$
σ_m^{GP}	$10\,mV$
θ_h^{GP}	$-58\,mV$
σ_h^{GP}	$12\,mV$
τ_{h0}^{GP}	$0.05\,ms$
τ_{h1}^{GP}	$0.27\,ms$
$\theta_{h\tau}^{GP}$	$-40\,mV$
$\sigma_{h\tau}^{GP}$	$12\,mV$
ϕ_h^{GP}	0.05

- Potasium current related parameters:

Parameter	Value
g_K^{GP}	$30\ \frac{nS}{(\mu m)^2}$
V_K^{GP}	$-80\,mV$
θ_n^{GP}	$-50\,mV$
σ_n^{GP}	$14\,mV$
τ_{n0}^{GP}	$0.05\,ms$
τ_{n1}^{GP}	$0.27\,ms$
$\theta_{n\tau}^{GP}$	$-40\,mV$
$\sigma_{n\tau}^{GP}$	$12\,mV$
ϕ_n^{GP}	0.05

- High-threshold calcium current related parameters:

Parameter	Value
g_{Ca}^{GP}	$0.1\ \frac{nS}{(\mu m)^2}$
V_{Ca}^{GP}	$120\,mV$
θ_s^{GP}	$-35\,mV$
σ_s^{GP}	$2\,mV$

- Low-threshold T-type calcium current related parameters:

Parameter	Value
g_T^{GP}	$0.5\ \frac{nS}{(\mu m)^2}$
θ_a^{GP}	$-57\,mV$
σ_a^{GP}	$2\,mV$
θ_r^{GP}	$-70\,mV$
σ_r^{GP}	$2\,mV$
τ_r^{GP}	$30\,ms$
ϕ_r^{GP}	1

- Calcium-activated voltage-independent "afterhyperpolarization" potasium current related parameters:

Parameter	Value
g_{AHP}^{GP}	$30\ \frac{nS}{(\mu m)^2}$
k_1^{GP}	30
k_{Ca}^{GP}	$20\ \frac{pA}{(\mu m)^2}$
$\epsilon_{x_{Ca}}^{GP}$	$1 \times 10^{-4}\ \frac{(\mu m)^2}{pA}(ms)^{-1}$

- Synaptic state-variables related parameters:

Parameter	Value
α^{GP}	2
θ_g^{GP}	$20\,mV$
θ_{gH}^{GP}	$-57\,mV$
σ_{gH}^{GP}	$2\,mV$

A.5.3 GPe cells' non-shared parameters

- Synaptic state-variables related parameter:

Parameter	Value
β^{GPe}	0.04

- Afferent synaptic currents related parameters:

Parameter	Value
$g_{GPe\rightarrow GPe}$	$1\ \frac{nS}{(\mu m)^2}$ (normal) ; $0\ \frac{nS}{(\mu m)^2}$ (Parkinsonian)
$V_{GPe\rightarrow GPe}$	$-80\,mV$
$g_{STN\rightarrow GPe}$	$0.3\ \frac{nS}{(\mu m)^2}$
$V_{STN\rightarrow GPe}$	$0\,mV$

- Constant current (used to multiply by the cell index number to create slight imbalance):

Parameter	Value
I_0^{GPe}	$0.3\ \frac{pA}{(\mu m)^2}$

- External applied current:

Parameter	Value
I_{app}^{GPe}	$-0.5\ \frac{pA}{(\mu m)^2}$ (normal) ; $-2.3\ \frac{pA}{(\mu m)^2}$ (Parkinsonian)

A.5.4 GPi cells' non-shared parameters

- Synaptic state-variables related parameters:

Parameter	Value
β^{GPi}	0.08

- Afferent synaptic currents related parameters:

Parameter	Value
$g_{STN\rightarrow GPi}$	$1\,\frac{nS}{(\mu m)^2}$
$V_{STN\rightarrow GPi}$	$0\,mV$
$\theta_{STN\rightarrow GPi}$	$0\,mV$

- External applied current:

Parameter	Value
I_{app}^{GPi}	$-1.2\,\frac{pA}{(\mu m)^2}$

A.5.5 Thalamic cells' parameters

- Membrane capacitance:

Parameter	Value
C_M^{Thl}	$1\,\frac{pF}{(\mu m)^2}$

- Leak current related parameters:

Parameter	Value
g_L^{Thl}	$0.05\,\frac{nS}{(\mu m)^2}$
V_L^{Thl}	$-70\,mV$

- Sodium current related parameters:

Parameter	Value
g_{Na}^{Thl}	$3\,\frac{nS}{(\mu m)^2}$
V_{Na}^{Thl}	$50\,mV$
θ_m^{Thl}	$-37\,mV$
σ_m^{Thl}	$7\,mV$
θ_h^{Thl}	$-41\,mV$
σ_h^{Thl}	$4\,mV$
a_{h0}^{Thl}	$0.128\,(ms)^{-1}$
θ_{ah}^{Thl}	$-46\,mV$
σ_{ah}^{Thl}	$18\,mV$
b_{h0}^{Thl}	$4\,(ms)^{-1}$
θ_{bh}^{Thl}	$-23\,mV$
σ_{bh}^{Thl}	$5\,mV$
ϕ_h^{Thl}	1

- Potasium current related parameters:

Parameter	Value
g_K^{Thl}	$5\,\frac{nS}{(\mu m)^2}$
V_K^{Thl}	$-90\,mV$

- Low-threshold T-type calcium current related parameters:

Parameter	Value
g_T^{Thl}	$5\,\frac{nS}{(\mu m)^2}$
V_T^{Thl}	$0\,mV$
θ_p^{Thl}	$-60\,mV$
σ_p^{Thl}	$6.2\,mV$
θ_r^{Thl}	$-84\,mV$ (but see note 1 below)
σ_r^{Thl}	$4\,mV$
τ_{r0}^{Thl}	$28\,ms$ (but see note 2 below)
τ_{r1}^{Thl}	$1\,ms$
$\theta_{r\tau}^{Thl}$	$-25\,mV$
$\sigma_{r\tau}^{Thl}$	$10.5\,mV$ (but see notes 1 and 2 below)
ϕ_r^{Thl}	2.5

Note 1: For the perturbation example we took $\theta_r^{Thl} = -79.8\,mV$ and $\sigma_{r\tau}^{Thl} = 11.025\,mV$.
Note 2: For the simulation of a "fast" T-current we took $\tau_{r0}^{Thl} = 5\,ms$ and $\sigma_{r\tau}^{Thl} = 15\,mV$.

- Afferent synaptic currents related parameters:

Parameter	Value
$g_{GPi\to Thl}$	$0.15\,\frac{nS}{(\mu m)^2}$
$V_{GPi\to Thl}$	$-85\,mV$

- Sensorimotor signal related parameters:

Parameter	Value
I_{SM}^{Thl}	$8\,\frac{pA}{(\mu m)^2}$
T_{SM}^{Thl}	$25\,ms$ (Terman's file) ; $50\,ms$ (Our simulations)
w_{SM}^{Thl}	$5\,ms$
d_{SM}^{Thl}	$80\,ms$

- Auxiliary sigmoidal function related parameter:

Parameter	Value
σ_Y	0.001

Acknowledgments: Special thanks go to Anne Beuter for her valuable contributions to this report and for her personal involvement in supporting this work. I would also like to thank Jacques Henry and Bedr'Eddine Ainseba for their guidance and mathematical advice during my internship. To all of them my most sincere gratitude for their long-lasting friendship. Finally, I would like to thank INRIA's International Internship Program for the financial support of this work.

References

[1] Rubin J. E. and Terman D. High frequency stimulation of the subthalamic nucleus eliminates pathological thalamic rhythmicity in a computational model. *J Comput Neurosci*, 2004, 16: 211–235.

[2] Benabid A. L., Pollak P., Louveau A., Henry S. and De Rougemont J. Combined (thalamotomy and stimulation) stereotactic surgery of the VIM thalamic nucleus for bilateral Parkinson's disease. *Appl Neurophysiol*, 1987, 50: 344–346.

[3] Benabid A. L., Pollak P., Gervason C., Hoffmann D., Gao D. M., Hommel M. et al. Long-term suppression of tremor by chronic stimulation of the ventral intermediate thalamic nucleus. *Lancet*, 1991, 337: 403–406.

[4] Chang, J.-Y. Brain Stimulation for Neurological and Psychiatric Disorders, Current Status and Future Direction. *J Pharmacol Exp Ther*, 2004, 309: 1–7.

[5] Titcombe M., Edwards R. and Beuter A. A mathematical approach to Parkinsonian tremor. *Nonlinear Studies*, 2004, 11: 363–384.

[6] Terman D., Rubin J. E., Yew A. C. Wilson C. J. Activity patterns in a model for the subthalamopallidal network of the basal ganglia. *J Neurosci*, 2002, 22: 2963–2976.

[7] Plenz D. and Kitai S. T. A basal ganglia pacemaker formed by the subthalamic nucleus and external globus pallidus. *Nature*, 1999, 400: 677–682.

[8] Garcia L., D'Allessandro G., Bioulac B. and Hammond C. High frequency stimulation in Parkinson's disease: more or less? *Trends Neurosci*, 2005, 28(4): 209–216.

[9] Grill W.M., Snyder A.N., Miocinovic S. Deep brain stimulation creates an informational lesion of the stimulated nucleus. *Neuroreport*, 2004, 15:1137-1140.

[10] Olanow W., Brin M. and Obeso J. The role of deep brain stimulation as a surgical treatment for Parkinson's disease. *Neurology*, 2000, 55(suppl. 6):S60–S66.

[11] Sohal V. and Huguenard J. Reciprocal inhibition controls the oscillatory state in thalamic networks. *Neurocomp.*, 2002, 44: 653–659.

[12] Bevan M. D. and Wilson C. J. Mechanisms underlying spontaneous oscillation and rythmic firing in rat subthalamic neurons. *J Neurosci*, 1999, 19:7617–7628.

[13] Bevan M. D., Wilson C. J., Bolam J. P., Magil P. J. Equilibrium potential of $GABA_A$ current and implications for rebound burst firing in rat subthalamic neurons in vitro. *J Neurophysiol*, 2000, 83:3169–3172.

[14] Kita H. and Kitai S. T. Intracellular study of rat globus pallidus neurons: membrane properties and responses to neostriatal, subthalamic and nigral stimulation. *Brain Res*, 1991, 564:296–305.

[15] Nambu A. and Linãs R. Electrophysiology of globus pallidus neurons in vitro. *J Neurophysiol*, 1994, 72:1127–1139.

[16] Cooper A. J. and Stanford I. M. Physiological and morphological characteristics of three types of rat globus pallidus neurone in vitro. *J Neurophysiol (Lond)*, 2000, 527:291–304.

[17] Ermentrout B. Simulating, Analyzing, and Animating Dynamical Systems. Philadelphia: SIAM Press, 2002.

[18] Lozano A. M., Dostrovsky J., Chen R. and Ashby P. Deep brain stimulation for Parkinson's disease: disrupting the disruption. *Lancet Neurol*, 2002, 1: 225–231.

Unité de recherche INRIA Futurs
Parc Club Orsay Université - ZAC des Vignes
4, rue Jacques Monod - 91893 ORSAY Cedex (France)

Unité de recherche INRIA Lorraine : LORIA, Technopôle de Nancy-Brabois - Campus scientifique
615, rue du Jardin Botanique - BP 101 - 54602 Villers-lès-Nancy Cedex (France)
Unité de recherche INRIA Rennes : IRISA, Campus universitaire de Beaulieu - 35042 Rennes Cedex (France)
Unité de recherche INRIA Rhône-Alpes : 655, avenue de l'Europe - 38334 Montbonnot Saint-Ismier (France)
Unité de recherche INRIA Rocquencourt : Domaine de Voluceau - Rocquencourt - BP 105 - 78153 Le Chesnay Cedex (France)
Unité de recherche INRIA Sophia Antipolis : 2004, route des Lucioles - BP 93 - 06902 Sophia Antipolis Cedex (France)

Éditeur
INRIA - Domaine de Voluceau - Rocquencourt, BP 105 - 78153 Le Chesnay Cedex (France)
http://www.inria.fr
ISSN 0249-6399